PAPER

Preparation of a porous graphite felt electrode for advance vanadium redox flow batteries†

Lei Zhang,‡[ab] Junpei Yue,‡[d] Qi Deng, [b] Wei Ling,[b] Chun-Jiao Zhou,[b] Xian-Xiang Zeng,[b] Congshan Zhou, *[a] Xiong-Wei Wu*[b] and YuPing Wu *[bc]

Rapid mass transfer and great electrochemical activity have become the critical points for designing electrodes in vanadium redox flow batteries (VRFBs). In this research, we show a porous graphite felt (GF@P) electrode to improve the electrochemical properties of VRFBs. The generation of pores on graphite felt electrodes is based on etching effects of iron to carbon. The voltage and energy efficiencies of VRFB based on the GF@P electrode can reach 72.6% and 70.7% at a current density of 200 mA cm^{-2}, respectively, which are 8.3% and 7.9% better than that of untreated GF@U (graphite felt). Further, the VRFBs based on GF@P electrodes possess supreme stability after over 500 charge–discharge cycles at 200 mA cm^{-2}. The high-efficiency approach reported in this study offers a new strategy for designing high-performance electrode materials applied in VRFBs.

1. Introduction

Exploiting large-scale energy storage technologies to accomplish highly-efficient utilization of renewable energy sources is becoming one of the hottest study fields.[1,2] Among them, vanadium redox flow batteries (VRFBs) possess many advantages including flexible capacity design, long cycle lifetime and environmental friendliness. Hence, they are considered as the most promising large-scale energy storage system, *e.g.* they have been equipped with a megawatt–hour-scale.

In spite of such great success, its low energy efficiency cannot compete with other electrochemical energy storage technologies, for instance lithium ion batteries, and finding approaches to enhance it is essentially important in the field. The electrodes, which offer sites for the vanadium-ion redox reactions, are regarded as the key for the high-efficiency VRFB. At present, the graphite felts are widely applied as electrode materials for VRFBs owing to their great stability and high conductivity under concentrated acidic conditions.[3] Their low catalytic activity and low specific surface area cannot facilitate and promote the

[a]College of Chemistry and Chemical Engineering, Hunan Institute of Science and Technology, Yueyang, Hunan 414006, China. E-mail: zhoucongsh@126.com

[b]School of Chemistry and Materials Science, Hunan Agricultural University, Changsha, Hunan 410128, China. E-mail: wxwcsu05@aliyun.com

[c]College of Energy and Institute for Advanced Materials, Nanjing Tech University, Nanjing, Jiangsu, 211816, China. E-mail: wuyp@fudan.edu.cn

[d]CAS Key Laboratory of Molecular Nanostructure and Nanotechnology, Institute of Chemistry, Chinese Academy ofSciences (CAS), Beijing 100190, China. E-mail: jpyue@iccas.ac.cn

† Electronic supplementary information (ESI) available. See DOI: 10.1039/d0ra00666a

‡ The authors equally contributed to this work.

redox process. Thus, various electrocatalysts are utilized to modify GF to enhance the redox process. For instance, some metal or metal oxides, such as Ir, Pt, Mn_3O_4, ZrO_2, *etc.*, were deposited on the surface of electrodes as catalysts and they can significantly promote the redox process.[4–7] However, precious metals are expensive and prone to promote hydrogen evolution; furthermore, the preparation process is tedious and complicated, limiting their further development. Recently, carbon-based electrocatalysts attracted more and more attentions. Compared with metal-modified GF materials, carbon-based materials are inexpensive and possess good stability under acidic conditions.[8] Moreover, most carbon-based catalyst materials have good electronic conductivity and high specific surface area, such as carbon nanotubes,[9] graphene oxides,[10] porous carbon,[11] and other categories.[12] Heteroatom doped carbon materials can promote the catalytic activity towards vanadium redox couples by offering the effective active surface sites and electron affinity.[13]

Additionally, maintaining the stability of the VFRB is another challenge due to the unavoidable decrease in catalytic activity or even mass loss of catalysts. From this standing view, modifying GF themselves to enable them with good catalytic activity is more reliable than decorating them with catalysts. Recently, the porous GF-based materials produced *via* thermal or KOH etching have been reported in lithium-ion batteries,[14] supercapacitors,[15] and VRFB.[16]

Herein, we present a simple and economical approach to prepare porous graphite felt (GF@P) for VRFB (illustrated in Fig. 1). The porous morphology of GF@P offers it a great surface area and further active sites for the electrochemical reaction of vanadium redox coupling. The porous structure can reduce the electrochemical polarization due to fast mass transportation.
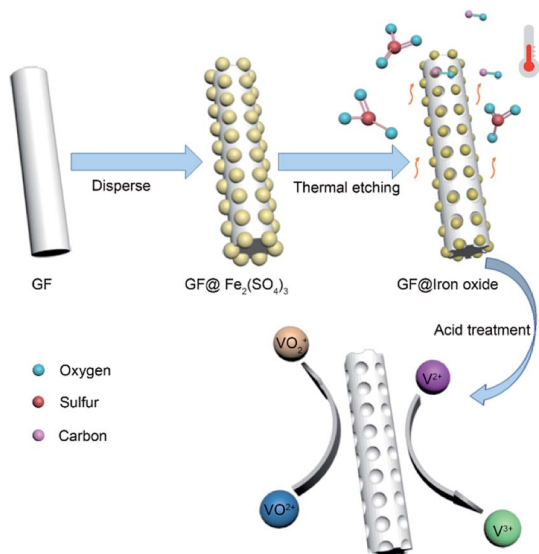
Fig. 1 Schematic of the preparation process of GF@P electrode.

Beneficial from this structure, the electrode shows enhanced electrochemical activity and reversibility in redox reactions along with stability at high current densities.

2. Results and discussion

In the process of scientific research, carbon is widely used as a reductant to extract metal from metal oxide ore. The related reaction is called carbon-thermal reduction. In this study, we used the carbon-thermal reduction to construct the proposed porous network-based GF@P electrode. The preparation process of the GF@P fiber electrode is shown in Fig. 1. The whole process can be expressed as follows:[11,17] (i) firstly, the thin layer of iron species precursors was coated onto the graphite felt surfaces; (ii) at the high temperature process, the precursors were transferred to iron oxides and subsequently such iron oxides went through carbon-thermal reduction and were reduced to iron species with low valences (this process consumes carbon species on graphite felt); (iii) finally, the iron species were removed with hydrochloric acid to left porous GF.

In order to confirm such process, the intermediate products were monitored and examined through SEM images and XRD (Fig. S4†) patterns. Their SEM images of the GF@U, GF@B, GF@A and GF@P are shown in Fig. 2. For the untreated graphite felts, their surface is smooth and clean, while it can be clearly observed that the surface is coated with iron species for GF@B (Fig. 2a and b). From EDS mapping (Fig. S1†), Fe, C, S, O can be found and the XRD pattern indicates the amorphous phase. It can be deduced that the iron species precursors partially hydrolyze to form amorphous phases. After heat treatment, the GF surfaces are covered by numerous small nanoparticles and EDS mapping shows the existence of only Fe, O, and C (Fig. S2†). Meanwhile, XRD pattern indicates the Fe_3O_4 phase. The existence of Fe^{2+} in Fe_3O_4 demonstrate the occurrence of carbon-thermal reduction. After removing iron species on the surface of GF by washing with HCl, numerous pores are
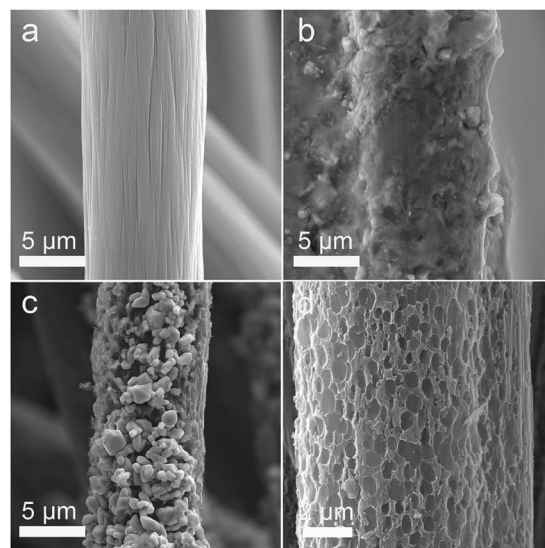

Fig. 2 The scanning electron microscope images of GF@U (a), GF@B (b), GF@A (c) and GF@P (d).

generated as expected (Fig. S3† and 2d). All these results perfectly confirm the abovementioned principle.

Raman spectroscopy is of great importance to examine the microstructure of carbon materials and the results are shown in Fig. 3a. Two vibration bands of carbon located at 1350 and 1600 cm^{-1}, which are attributed to D and G peaks. The intensity
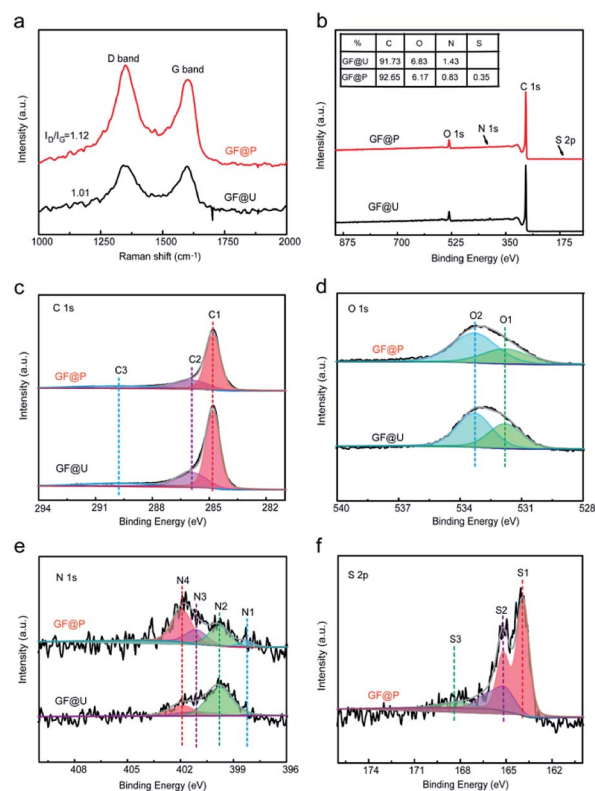

Fig. 3 (a) Raman spectra of GF@U and GF@P of electrode materials. (b) XPS spectra of GF@U and GF@P. (c–f) High-resolution of C1s, O1s, N1s and S2p for GF@U and GF@P.

ratio of D and G peaks (I_D/I_G) can reflect the defect degree carbon materials. Compared with untreated GF, the abovementioned processes not only create porous on their surface but also increase defects, which can be confirmed from the increased I_D/I_G ratio (from 1.01 to 1.12). These defects can provide the abundant active sites for redox process (VO^{2+}/VO_2^+ and V^{3+}/V^{2+}). In order to further understand the atomic environments of carbon, XPS measurements were carried out on these two materials, as shown in Fig. 3. Aside from C, O, and N, the signal of S2p can be found in GF@P, as marked in Fig. 3b. The sulfur can be derived from the iron precursors species. Interestingly, the contents of O and N in GF@P get less than the pristine GF@U, which may be caused by the thermal reduction at high temperature as well. The chemical environments and chemical bonding of these atoms are analyzed *via* their core level XPS. In order to calibrate the charge effects, the binding energy of C–C bonds was shifted to 284.8 eV. C1s bands can be deconvoluted into three peaks: 284.8 (C1), 285.9 (C2), and 289.8 (C3) eV, which can be contributed to C–C/C–H, C=N/C–N, and O–C=O, respectively. It can be clearly seen that the contents of C=O/C–N and O=C–O get less for GF@P, in good agreement with the XPS survey results.[18,19] The O 1s peak Fig. 3d was divided into two peaks, mainly from C–OH (O2, 533.3 eV) and C=O or O=C–N (O1, 531.8 eV) groups.[20] It can be seen from Fig. 3e that nitrogen elements can be composed of four characteristic peaks, N4 (401.9), N3 (401.1 eV), N2 (399.8 eV), and N1 (398.3 eV), which can be attributed to oxygenated-N, graphitic-N, pyrrolic-N, and pyridinic-N, respectively.[21] Simultaneously, the high-resolution S2p spectra (Fig. 3f) exhibited three main peaks at 167.8 (S3), 165.1 (S2), and 163.9 (S1) eV, which can be assigned to –C–SOx, –C–SOy, C–S, respectively.[22] Sulfur doping is conducive to mutual conversion between V^{2+}/V^{3+} and VO^{2+}/VO_2^+.[23] The porous morphology of the electrode surface promotes vanadium ion diffusion, and then the C–OH, pyridinic N and pyrrolic N on the electrode surface provide active sites for vanadium redox reaction. Finally, the sulfur element can form S–O–V transition state with the vanadium and accelerate the vanadium ion conversion. So these factors together improve the performance of the battery.[10,12,22]

The effects of such treatment on electrochemical performance of GF electrodes for VRFB were examined using cyclic voltammetry in a three-electrode system, shown in Fig. 4a and b. It can be clearly observed that the anodic and cathodic peak potential difference (ΔE) for V^{3+}/V^{2+} and VO_2^+/VO^{2+} using GF@P are 279 and 330 mV, respectively. These values are significantly less than the ones using GF@U electrode. The related parameters are listed in Table S1.† The decrease in potential separation demonstrates the small polarization for redox process and the fast kinetic process. The fast kinetic process of redox couples on GF@P electrodes may be originated from the high surface area and high electrocatalytic activity from heteroatom doping, as shown in SEM and XPS spectra. In addition, for the redox couple of V^{3+}/V^{2+} the one using GF@U electrode showed no obvious redox peak when compared with the one using GF@P electrode, which may be due to the relatively weak catalysis of GF@U electrode to V^{2+}/V^{3+} ion conversion and the occurrence of hydrogen evolution reaction. All these results

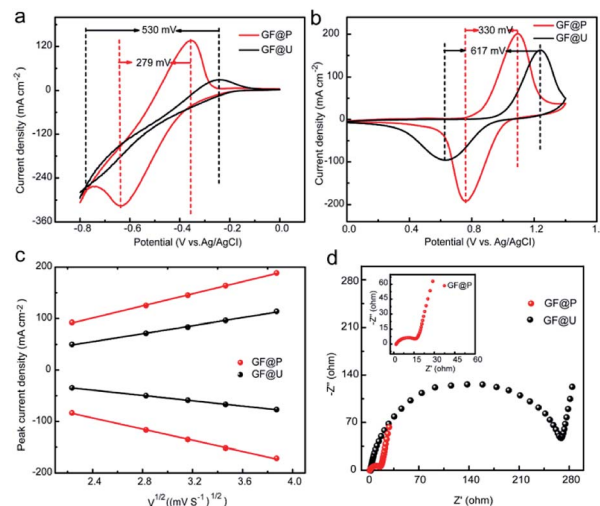**Fig. 4** (a) and (b) Cyclic voltammetries of V^{3+}/V^{2+} and VO^{2+}/VO_2^+ redox using GF@U and GF@P electrodes at a scan rate of 10 mV s^{-1}. (c) The relationship between GF@U and GF@P peak current density and square root of sweep speed. (d) Impedance diagram of GF@U and GF@P.

confirm, GF@P electrodes present excellent catalytic activity for both V^{2+}/V^{3+} and VO^{2+}/VO_2^+ redox couples.

In order to understand the detailed kinetic process, scanning rate dependent CVs are carried out and shown in Fig. S5.† The ratio of $-I_{pc}/I_{pa}$ for the VO^{2+}/VO_2^+ redox reaction using GF@U and GF@P electrodes at different sweep rates are shown in Fig. S6.† Compared with the blank GF (0.706), the value for GF@P (0.932) is close to 1, indicating the high reversibility. Moreover, the sweep rate does not change the ratio too much for GF@P, indicating the much improved kinetic process. Furthermore, the good linear relationship between i_p and the square root of the scanning rates ($\nu^{1/2}$) (Fig. 4c) shows that the diffusion process controls the electrochemical reaction of the VO^{2+}/VO_2^+ couple. For the electrochemically reversible process, Randles Sevcik equation can be used to estimate the diffusion coefficient.[24]

$$i_p = 2.99 \times 10^5 \alpha^{1/2} A n^{3/2} D_0^{1/2} \nu^{1/2} C_0. \tag{1}$$

where i_p represents the peak current density, α stands for the charge transfer coefficient, A denotes the effective area of the electrode, n denotes the number of electrons transferred in electrochemical reaction, ν is for the scan rate, D_0 expresses the diffusion coefficient, C_0 is the concentration of the active substance. Hence, the diffusion rate of vanadium on the electrode can be examined from the slope of the peak current to the square root of the scanning rate. The slopes of the oxidation and reduction processes on the GF@P are 58.53 and 54.75, respectively, which are much larger than those of GF@U (38.45, 26.56), indicating that the mass diffusion process on the porous electrode is faster. Moreover, the kinetic process of the reaction was examined by electrochemical impedance spectra, seeing Fig. 4b. It can be seen that Nyquist plot mainly comprises a semicircle in the high-frequency area and diagonal line in the low-frequency area, which reflects the information for the charge transfer
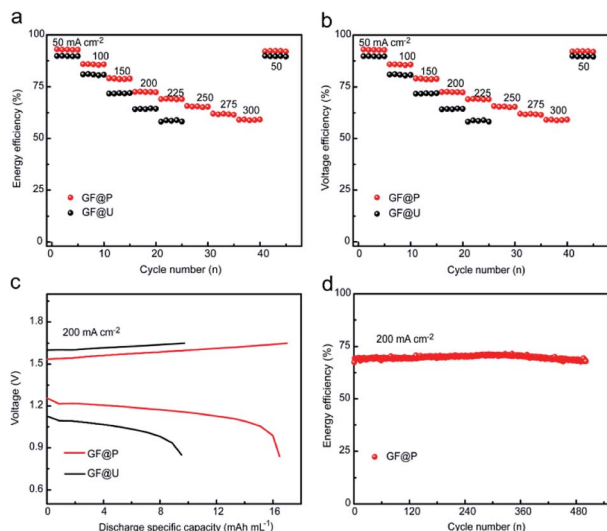
Fig. 5 Charge and discharge performance of VRFBs using GF@U and GF@P electrodes. (a) Energy efficiency. (b) Voltage efficiency. (c) Charge–discharge curves of VRFBs at current density of 200 mA cm⁻². (d) Long cycle test of GF@P assembled batteries at 200 mA cm⁻².

process and diffusion information and can fitted through a simple equivalent circuit: $R_s - R_{ct}/Q - W$ (R_s denotes the solution resistance, R_{ct} denotes charge transfer resistance, and W is the Warburg impedance).[20] The R_{ct} value of the GF@U is approximately 270 Ω, 19 times higher than the one (15 Ω) GF@P electrodes, suggesting that the vanadium-ion redox reaction is more likely to happen in the GF@P electrode. The impedance results were also confirmed by CV.

Furthermore, the flow batteries based GF@P electrodes were assembled and evaluated, as shown in Fig. 5. The charge and discharge curves of VRFBs using GF@U and GF@P electrodes at the current density of 200 mA cm⁻² (Fig. 5c) confirmed the small potential polarization when using GF@P electrodes again. In addition, it can be clearly seen from Fig. S7† that GF@P battery shows a lower charging and discharging over-potential and has a higher charging and discharging capacity. This small polarization can stand for the application of high current density, *e.g.* more than 300 mA cm⁻² when using GF@P while this value is only 225 mA cm⁻² for GF@U. Furthermore, the voltage and energy efficiencies of the battery using GF@P electrode at 200 mA cm⁻² are 72.6% and 70.7%, respectively, each of which increases by 8.3% and 7.9% compared with GF@U. The cycling stability was evaluated as well and the energy efficiency at 200 mA cm⁻² of VRFBs using GF@P electrodes maintain very stable after 500 cycles. These excellent electrochemical performances confirm the success of porous electrode design, which works as good electrocatalytic activity, promotes mass diffusion, increase the cycling lifetime.

3. Experiment

3.1 Preparation of GF@P

Firstly, GF (3 × 4 cm²) was immersed in 50 mL 1.6 mol L⁻¹ ferric sulfate solution. The resulted samples were then dried at 60 °C

for 12 hours. Next, the modified GF was annealed in N2 atmosphere at 900 °C for 3 h with a heating rate of 5 °C min⁻¹. Finally, the activated GF was soaked in concentrated hydrochloric acid to dissolve oxides and obtain porous graphite felt. The resulted GF was referred to as GF@P and untreated GF was referred to as GF@U. In order to better observe the changes of graphite felt in the reaction process, the graphite felts before and after the heat treatment were named GF@B and GF@A, respectively. All samples were repeatedly rinsed with deionized water before testing.

3.2 Characterization

The morphology of the sample was observed by field emission scanning electron microscope (Tescan Mira3) under 15 kV and graphitisation degree and defects of the electrode materials were studied by Raman spectroscopy (LabRAM HR Evolution) using 532 nm laser excitation. The Elemental composition of the electrode materials was determined using X-ray photoelectron spectroscopy (XPS) using an EscaLab 250Xi equipped with a 200 W Al-Kα radiation source. The crystallinity of samples was detected by XRD in the condition of Cu Kα radiation (40 kV, 40 mA, 10° min⁻¹ from 10 to 80°).

3.3 Electrochemical measurement

The electrochemical properties of the three-electrode systems were tested using Ag/AgCl as a reference electrode, platinum network as the counter electrode, and graphite felt (0.5 × 0.5 cm⁻²) as the working electrode. Cyclic voltammetry was tested in the range of −0.8–1.4 V with different scanning rates the CHI604E electrochemical workstation. Electrochemical impedance spectra measurements were carried out with a voltage amplitude of 5 mV and a frequency scope of 0.01 Hz to 100 kHz. An aqueous solution with 0.1 M $VOSO_4$ and 3 M H_2SO_4 was used as the electrolyte for these measurements. For VRFB, the vanadium battery Nafion 115 membrane was used as an ion-exchange membrane and the size of graphite felt electrode used is 2 × 2 cm². 15 mL electrolytes composed of 1.5 M V^{3+}, 1.5 M $VOSO_4$, 3 M H_2SO_4 solution was circulated though the electrodes with the flow velocity of 40 mL min⁻¹ using a peristaltic pump. The charge–discharge profiles were collected on Land electrochemical systems (Land CT2001A) with cut-off voltage of approximately 0.8–1.65 V, which can prevent the high-voltage corrosion of the graphite plate and electrode.

4. Conclusions

In conclusion, we have successfully prepared porous GF electrodes using chemical etching. The formation of uniform pores significantly increased the specific surface area of the electrode, supplying more active sites for the redox reaction of vanadium ions, thus improving its electrochemical activity and kinetic reversibility. The discharge-specific capacity of the VRFB assembled with GF@P electrode was higher than that of the GF@U electrode. Under the high current density of 200 mA cm⁻², the VRFB with the GF@P electrode can work for 500 cycles without a significant attenuation, showing excellent rate

performance and ultra-long cycle stability. The method employed in this study can be extended to other carbon-based electrodes. It provides a new way to prepare various electrodes and has a broad application prospect in the energy storage and conversion processes.

Conflicts of interest

The authors declare no conflict of interest.

Acknowledgements

Notes and references

1 X. Ke, J. M. Prahl, J. I. D. Alexander, J. S. Wainright, T. A. Zawodzinski and R. F. Savinell, *Chem. Soc. Rev.*, 2018, **47**, 8721–8743.

2 S. Hennessey and P. Farràs, *Chem.Commun.*, 2018, **54**, 6662–6680.

3 P. C. Ghimire, R. Schweiss, G. G. Scherer, N. Wai, T. M. Lim, A. Bhattarai, T. D. Nguyen and Q. Yan, *J. Mater. Chem. A*, 2018, **6**, 6625–6632.

4 H. Zhou, Y. Shen, J. Xi, X. Qiu and L. Chen, *ACS Appl. Mater. Interfaces*, 2016, **8**, 15369–15378.

5 C. Flox, J. Rubio-Garcia, R. Nafria, R. Zamani, M. Skoumal, T. Andreu, J. Arbiol, A. Cabot and J. R. Morante, *Carbon*, 2012, **50**, 2372–2374.

6 Z. He, L. Dai, S. Liu, L. Wang and C. Li, *Electrochimi. Acta*, 2015, **176**, 1434–1440.

7 W. H. Wang and X. D. Wang, *Electrochimi. Acta*, 2007, **52**, 6755–6762.

8 Y. Xiang and W. A. Daoud, *J. Mater. Chem. A*, 2019, **7**, 5589–5600.

9 Y. Chung, C. Noh and Y. Kwon, *J. Power Sources*, 2019, **438**, 227063.

10 Q. Deng, P. Huang, W. X. Zhou, Q. Ma, N. Zhou, H. Xie, W. Ling, C.-J. Zhou, Y. X. Yin, X. W. Wu, X. Y. Lu and Y. G. Guo, *Adv. Energy Mater.*, 2017, **7**, 1700461.

11 Y. Liu, Y. Shen, L. Yu, L. Liu, F. Liang, X. Qiu and J. Xi, *Nano Energy*, 2018, **43**, 55–62.

12 Q. Ma, X. X. Zeng, C. Zhou, Q. Deng, P. F. Wang, T. T. Zuo, X. D. Zhang, Y. X. Yin, X. Wu, L. Y. Chai and Y. G. Guo, *ACS Appl. Mater. Interfaces*, 2018, **10**, 22381–22388.

13 R. Wang and Y. Li, *J. Power Sources*, 2019, **421**, 139–146.

14 M. S. Balogun, W. Qiu, F. Lyu, Y. Luo, H. Meng, J. Li, W. Mai, L. Mai and Y. Tong, *Nano Energy*, 2016, **26**, 446–455.

15 T. Li, W. Zhang, L. Zhi, H. Yu, L. Dang, F. Shi, H. Xu, F. Hu, Z. Liu, Z. Lei and J. Qiu, *Nano Energy*, 2016, **30**, 9–17.

16 T. Liu, X. Li, C. Xu and H. Zhang, *ACS Appl. Mater. Interfaces*, 2017, **9**, 4626–4633.

17 H. Wu, J. B. Jespersen, F. J. Frandsen, P. Glarborg, M. Aho, K. Paakkinen and R. Taipale, *AIChE J.*, 2013, **59**, 4314–4324.

18 P. Han, Y. Yue, Z. Liu, W. Xu, L. Zhang, H. Xu, S. Dong and G. Cui, *Energy Environ. Sci.*, 2011, **4**, 4710.

19 Z. He, Y. Jiang, Y. Wei, C. Zhao, F. Jiang, L. Li, H. Zhou, W. Meng, L. Wang and L. Dai, *Electrochimi. Acta*, 2018, **259**, 122–130.

20 H. Sheng, Q. Ma, J. G. Yu, X. D. Zhang, W. Zhang, Y. X. Yin, X. Wu, X. X. Zeng and Y. G. Guo, *ACS Appl. Mater. Interfaces*, 2018, **10**, 38922–38927.

21 Y. Gao, H. Wang, Q. Ma, A. Wu, W. Zhang, C. Zhang, Z. Chen, X. X. Zeng, X. Wu and Y. Wu, *Carbon*, 2019, **148**, 9–15.

22 Y. Xie, Z. Meng, T. Cai and W. Q. Han, *ACS Appl. Mater. Interfaces*, 2015, **7**, 25202–25210.

23 A. B. Shah, Y. Wu and Y. L. Joo, *Electrochimi. Acta*, 2019, **297**, 905–915.

24 W. Ling, Z. A. Wang, Q. Ma, Q. Deng, J. F. Tang, L. Deng, L. H. Zhu, X. W. Wu, J. P. Yue and Y. G. Guo, *Chem. Commun.*, 2019, **55**, 11515–11518.